Influence of deposition conditions on long-range electronic disorder in *n*-type doped hydrogenated amorphous silicon

D. Quicker and J. Kakalios
School of Physics and Astronomy, University of Minnesota, Minneapolis, Minnesota 55455
(Received 31 July 1998; revised manuscript received 18 March 1999)

Measurements of the conductivity, thermopower, and infrared absorption for *n*-type doped hydrogenated amorphous silicon (*a*-Si:H) films grown under varying deposition conditions have been performed, in order to test the role that compositional fluctuations associated with the bonded hydrogen microstructure have on the long-range disorder present at the conduction-band edge. Films grown either with high deposition power or at low substrate temperature have a lower conductivity and more long-range disorder of the mobility edge, as measured by the difference in the activation energies of the conductivity and thermopower. The long-range disorder (measured by the activation energy difference) is larger for films with a larger fraction of Si═H_2 bonds, as inferred from the infrared absorption, indicating that the hydrogen bonding is related to long-range electronic disorder. Computer simulations have also been performed in order to test the proposal that long-range disorder is responsible for the difference in the conductivity and thermopower activation energies. [S0163-1829(99)08027-3]

I. INTRODUCTION

It is well known that amorphous semiconductors such as hydrogenated amorphous silicon (*a*-Si:H) exhibit different thermal activation energies for the electrical conductivity and the thermopower. Several models have been proposed to account for this discrepancy,[1–3] with the long-range fluctuation model being the most widely accepted. In this model, the energy level of the conduction-band edge E_C varies by up to several hundred meV in space over length scales of $\sim 10^3$ Å, due to Coulombic potential fluctuations from charged dopants and defects, and possibly also structural inhomogeneities. Since the conductivity depends on the energy $E_C - E_F$ exponentially while the thermopower has a linear dependence on this quantity, a measurement of a macroscopic sample volume results in different averaging procedures for these properties, and thus a difference in activation energies.[4] The theory of long-range Coulombic potential fluctuations is well developed,[5,6] and these fluctuations are likely to play a significant role in doped *a*-Si:H. Extensive experimental studies of singly doped *n* and *p*-type *a*-Si:H, as well as compensated films containing both phosphorus and boron,[7–9] find an increase in the activation energy difference with doping level. However, structural and compositional inhomogeneities are also known to exist in *a*-Si:H, and their role in determining electronic transport properties is not as well understood.

Evidence of spatial fluctuations of the band gap of *a*-SiN_x:H has been found in the optical absorption of those materials,[10] and band-gap fluctuations have been used to model the density of states in *a*-Si:H.[11] In *a*-Si:H, nuclear magnetic resonance measurements have found a dilute phase of isolated Si—H bonds, and a clustered phase of approximately six hydrogen atoms in close proximity.[12] Moreover, infrared spectroscopy measurements demonstrate the presence of silicon-dihydride configurations (Si═H_2) characterized by an absorption band near 2100 cm^{-1} in addition to the silicon-monohydride (Si—H) absorption band at 2000 cm^{-1}. Both the amount of hydrogen in the clustered phase and in the Si═H_2 bonding configurations increase when the growth conditions of the *a*-Si:H films are varied to produce material with lower electronic quality. It is likely that regions of the sample with larger hydrogen content will have larger local band gaps,[13] causing additional modulations of the mobility edge beyond the potential fluctuations induced by charged defects or impurities, but the exact nature of this effect is not known, nor has the influence of hydrogen microstructure on the long-range disorder been experimentally investigated.

To study the effects of structural disorder, we have measured the conductivity and thermopower for a series of samples deposited with identical doping levels but different growth conditions. The hydrogen bonding in these films is also measured using infrared spectroscopy. While studies of the influence of varying deposition conditions and the corresponding infrared spectra for *a*-Si:H have been reported before,[14–16] to our knowledge what is new about this work is the careful assessment of the activation energy difference E_Δ as the growth conditions are varied, and the correlation of E_Δ with the hydrogen microstructure. In addition, computer simulations of random resistor networks are described which further support the identification of E_Δ as a measure of the long-range disorder of the electronic transport states.

II. EXPERIMENTAL METHODS

The samples studied here were synthesized using plasma-enhanced chemical vapor deposition (PECVD) of SiH_4 and PH_3 (for *n*-type doping) in a capacitively coupled rf (13.56 MHz) system at the University of Minnesota. The films used in this study were deposited with a gas-phase doping ratio of $[PH_3]/[SiH_4] = 4 \times 10^{-4}$. For one series of samples, the rf power was held constant at 3 W (electrode area ~ 50 cm^2) while the deposition temperature was varied from 250 °C down to room temperature (≈ 22 °C). For another series of

films the rf power used during the deposition was varied from 1 to 90 W, while the deposition temperature was held constant at 250 °C. For conductivity and thermopower measurements, two chromium coplanar electrodes ~500 Å thick with a separation of 4 mm are deposited onto each sample. The sample is mounted inside a shielded vacuum chamber across two independently heated and controlled copper blocks; so that one electrode is above each block. A type-T thermocouple is attached with silver paint to the inner edge of each electrode to measure the temperature on each side of the sample. Wires are attached to the chromium electrodes using indium, and these connections are used to measure both the conductivity and thermopower. For a given average temperature, the thermopower is calculated by measuring the slope of a plot of the thermoelectric voltage as a function of temperature difference ΔT, for several values of ΔT in the range ± 6 °C (Ref. 17).

Infrared-absorption spectra were measured using a Nicolet Magna 750 Fourier-transform infrared spectrometer, over the spectral range from 400 to 4000 cm^{-1}, while the sample is in a dry nitrogen environment. The absorption $\alpha(\omega)$ of the a-Si:H film is calculated by dividing out the background of a blank crystalline Si substrate measured under the same conditions. Over the spectral range from 1800 to 2250 cm^{-1}, we perform a least-squares fit to two Gaussian distributions centered near $\omega \approx 2000$ and 2100 cm^{-1} (with the peak positions allowed to vary), and then calculate the microstructure fraction[16]

$$R = \frac{I_{2100}}{I_{2000} + I_{2100}}, \tag{1}$$

where I_{2000} and I_{2100} are the integrated areas under the Gaussian curves centered at wave numbers 2000 and 2100 cm^{-1}, respectively. Consistent and reproducible fits to the infrared spectra are obtained when the same widths are used for both Gaussian distributions (which also decreases the number of adjustable parameters in the fit).

III. EXPERIMENTAL DATA AND ANALYSIS

A. Varying deposition temperature

It is well known that a-Si:H films grown by PECVD show the highest quality electronic properties when the substrate temperature T_S during deposition is between 200 and 300 °C, and low rf power levels (corresponding to deposition rates of 1–3 Å/sec) are used. Samples deposited at lower temperatures or higher power levels generally have higher defect densities, higher hydrogen content, more pronounced hydrogen microstructure, and lower conductivity.[18,19] As expected, our low-T_S films show greatly reduced electrical conductivity (up to seven orders of magnitude lower) when compared to a-Si:H deposited at 250 °C. The conductivity of these low-T_S samples increased as the films were annealed at higher temperatures, although the conductivity never reached the values found in a $T_S = 250$ °C sample. In Fig. 1 the conductivity (measured upon heating) of the sample deposited at 60 °C is plotted as a function of inverse temperature in the as-deposited state as well as after 2 h of annealing at 100, 150, and 200 °C. The room-temperature conductivity of films grown at $T_S < 150$ °C increased by approximately three orders of magnitude, with the largest change occurring between the anneals at 100 and 150 °C. Figure 2 shows the temperature dependence of the conductivity for the entire series of samples, after they were all annealed at 200 °C for 2 h. Even following this anneal, the films deposited at low substrate temperatures remain much less conductive than even the sample which was deposited at 150 °C (for which annealing hardly affected the conductivity). Clearly some of the disorder introduced during deposition is fixed and cannot be altered with subsequent thermal treatments.

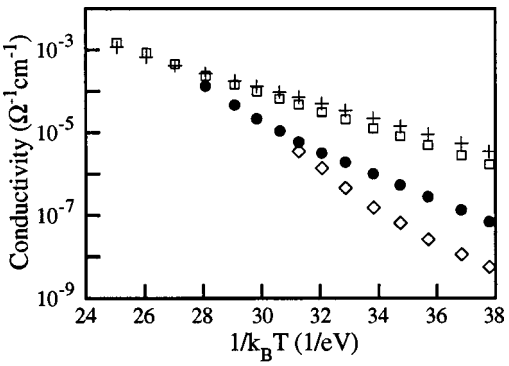

FIG. 1. Arhennius plot of the conductivity of the sample deposited at $T_S = 60$ °C in the as-deposited state (open diamonds) and after annealing at 100 °C (solid circles), 150 °C (open squares), and 200 °C (+ marks).

Thermal equilibration, a well known phenomenon in a-Si:H believed to result from hydrogen motion, is reflected by kinks in Arhennius plots of the conductivity, indicated by the arrows in Fig. 2 for samples deposited at 80 °C and higher. Thermal equilibration has been found to depend on the deposition power,[20] and a similar behavior is observed here in films grown at lower substrate temperatures, suggesting that the underlying hydrogen motion becomes slower as the deposition temperature is lowered.

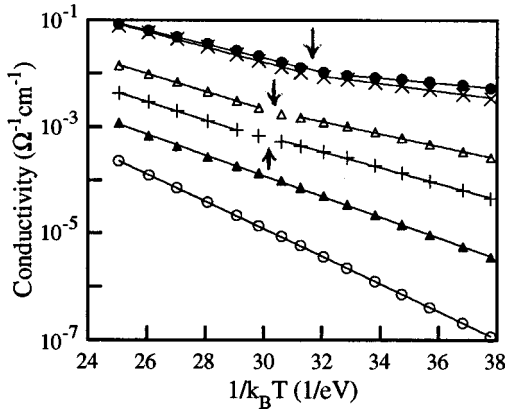

FIG. 2. Arhennius plot of the conductivity of the entire series of samples deposited with varying substrate temperature, after each had been annealed at 200 °C for 2 h. The samples are as follows: solid circles for $T_S = 250$ °C, crosses for 150 °C, open triangles for 100 °C, + marks for 80 °C, solid triangles for 60 °C, and open circles for 22 °C. The lines are exponential fits to the conductivity above and below the equilibration temperature, which is marked by an arrow for the samples deposited at $T_S = 250$, 150, 100, and 80 °C.

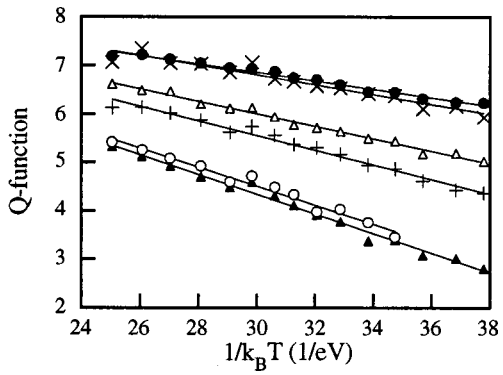

FIG. 3. Plot of the Q function against inverse temperature for the entire series of films deposited with varying substrate temperature, after annealing at 200 °C for 2 h (using the same symbols as Fig. 2). The lines are fit to the data using Eq. (5).

The thermopower has also been measured for these films, both before and after annealing when possible. The samples deposited at the lowest substrate temperatures were initially too resistive for accurate thermopower measurements, but could be studied after annealing at 100 °C or higher. For any *n*-type material with a sharp mobility edge, the thermopower should be given by[21]

$$S=-\frac{k_B}{e}\left(\frac{E_C-E_F}{k_BT}+A\right), \tag{2}$$

where A is independent of temperature. For all samples studied here, E_C-E_F measured from the thermopower is less than the activation energy E_C-E_F obtained from the conductivity

$$\sigma=\sigma_0\exp\left(-\frac{E_C-E_F}{k_BT}\right). \tag{3}$$

This discrepancy is observed quite generally in amorphous semiconductors,[6,8] and has been ascribed to the influence of long-range disorder on the electronic transport states.[3] To compare the conductivity and thermopower without the influence of the statistical shift of E_F, Beyer, Fischer, and Overhof proposed the function[22]

$$Q=\frac{e}{k_B}|S|+\ln[\sigma(\Omega\ \mathrm{cm})]. \tag{4}$$

The Q function is independent of the position of E_F and of temperature if σ and S have the same activation energy. The slope of the Q function for the 60 °C sample in Fig. 1 decreased when the film was initially heated above 100 °C, but hardly changed for annealings between the 150 and 200 °C. Similar behavior was observed in the other films. Figure 3 shows the Q function for all samples after annealing at 200 °C. The data for each sample are fit to the expression

$$Q=Q_0-E_\Delta/k_BT. \tag{5}$$

We find that the value of E_Δ, which equals the difference between the conductivity and thermopower activation energies, increases from 0.09 eV for the sample deposited at 250 °C, to 0.20 eV for the sample deposited at room temperature, while the Q_0 values are 9–11 for all the films in Fig. 3. Typical uncertainties for E_Δ are ±10%. Our value of 0.09 eV for the $T_S=250$ °C sample is slightly lower than the activation energy difference of 0.12 eV obtained by Beyer and co-workers[7,3] for films of similar doping levels in 1977, perhaps indicating a difference in sample quality. The values of E_Δ for each film are listed in Table I. These results will be discussed further in Sec. V of this paper.

The infrared absorption in the 2000–2200-cm^{-1} range depends strongly on the deposition temperature, as observed in previous reports.[14,15] The sample deposited at 250 °C has an R value [calculated from Eq. (1)] of 0.17, while the room-temperature substrate film has $R=0.82$. The value of R for each sample in the as-deposited state and after annealing at 200 °C is listed in Table I. Uncertainties in the values of R are approximately ±0.04.

B. Varying deposition power

A series of *n*-type doped *a*-Si:H films all synthesized at 250 °C, but with varying rf power during deposition, was also studied. The samples deposited using a rf power of 10 W or less had the highest conductivities and the lowest values of E_Δ, while a rf power of 20 W or higher resulted in a lower conductivity and a higher E_Δ, indicating more disorder. The infrared absorption also changed systematically with deposition power, exhibiting an increased microstructure fraction R at higher power levels. The values of E_Δ and R, as well as the deposition rate, are listed in Table II. Also listed in Table II (marked by an asterisk next to their power level) are data for three samples that were grown with a slightly different configuration in the deposition chamber. For these films an extender was used to increase the separation between the anode and cathode to approximately 3 in. instead of approximately 1 in. for all of the other samples. This modification serves to move the substrate away from the most intense region of the plasma, significantly reducing

TABLE I. Silicon dihydride relative concentration (R) and activation energy difference (E_Δ) as a function of deposition temperature.

Deposition temperature (°C)	R (as deposited)	R (annealed at 200 °C)	E_Δ (eV) (annealed at 200 °C)
250	0.17	0.18	0.087
150	0.32	0.33	0.101
100	0.60	0.56	0.129
80	0.61	0.66	0.150
60	0.72	0.73	0.204
22	0.82	0.85	0.197

TABLE II. Deposition rate, silicon dihydride relative concentration (R), and activation energy difference (E_Δ) as a function of rf power during film growth. The samples marked with an asterisk used a different growth configuration, as described in the text.

rf power (W)	Deposition rate (Å/s)	R	E_Δ (eV)
1	1.6	0.19	0.095
3	2.2	0.17	0.084
10	5.6	0.24	0.082
25	11	0.32	0.103
40	23	0.34	0.109
60	29	0.36	0.111
90	33	0.35	0.110
10*	0.7	0.26	0.082
20*	1.3	0.44	0.101
50*	5.3	0.69	0.152

the deposition rate for a given power level. However, it also tends to increase the amount of dust generated during the deposition process. As seen in Table II, the samples deposited in this manner have more hydrogen microstructure, as reflected by higher R values. The 50-W sample deposited with the extender also has a significantly larger E_Δ than the other films in this series, even though its deposition rate is similar to the 10-W sample in the normal configuration. These results demonstrate that even if the deposition temperature and deposition rate are held constant, the sample properties are sensitive to the detailed nature of the deposition process.

C. Analysis

Figure 4 shows a plot of the activation energy difference E_Δ as a function of the microstructure fraction R for all of the films studied here. A good correlation between these quantities can be seen, where samples with large values of R (higher Si═H_2 content) generally also exhibit large values of E_Δ. Although the samples deposited with varying rf powers (with and without the extender) do not cover as wide a range

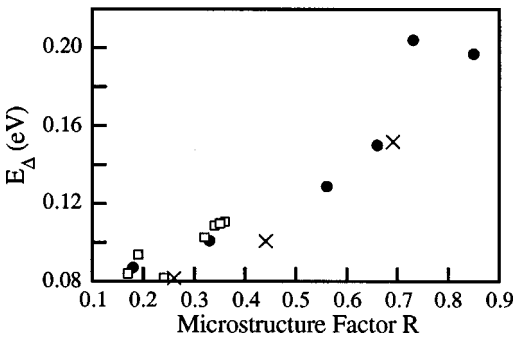

FIG. 4. Plot of E_Δ [calculated from Eq. (5)] as a function of the microstructure fraction R [calculated from Eq. (1)] for all of the films studied here. The open squares are for the samples deposited with varying rf power, crosses are for the samples deposited with the extender, and solid circles are for the samples deposited with varying substrate temperature (after being annealed at 200 °C for 2 h.).

as the samples deposited with varying substrate temperature, the correlations between E_Δ and R are quite similar for all three series of films. This supports the idea that structural disorder can be responsible for the difference in activation energies. It also suggests that Si═H_2 bonding in the amorphous silicon network either directly adds to the long-range disorder of the mobility edge, or that the Si═H_2 bonding and long-range disorder have a common origin. We note that extrapolating the data in Fig. 4 to $R=0$ still leads to a nonzero value of E_Δ, which would presumably be due to the Coulombic potential fluctuations from charged dopants and defects and the intrinsic hydrogen microstructure that is found even when no Si═H_2 is present.

IV. COMPUTER SIMULATIONS

Computer simulations of the conductivity and thermopower of random resistor lattices were previously performed by Overhof and Beyer.[3] These authors calculated the conductivity by directly inverting Kirchoff's equations for the entire resistor network, and then calculated the Peltier heat in the same way and used Onsager's relation to obtain the thermopower. Because of the large computational effort required, they used lattices of $10\times10\times10$ (in three dimensions) or 40×40 (in two dimensions) or smaller. As a source of disorder they used Coulomb potentials generated by a random distribution of point charges. We have performed simulations of random resistor networks, using a different method which allows for the direct calculation of both the conductivity and thermopower. This procedure is computationally more efficient so that larger lattices could be calculated. In addition, more general types of disorder were also examined.

To represent the spatial fluctuations of the mobility edge in these simulations each point of a two-dimensional square lattice is assigned an activation energy (which would equal E_C-E_F) using one of several different methods described below. Each point was connected to each of its four nearest neighbors via a bond which is assigned an activation energy equal to the average energies of the two points it connects. It was assumed that this activation energy would be the same for the thermopower and conductivity [as in Eqs. (2) and (3)] on this microscopic scale. Across each bond, Ohm's law $\Delta V=IR$ and the relation $S=\Delta V/\Delta T$ were assumed to hold, allowing the derivation of an expression for the current through each bond as a function of its activation energy and the potential difference and temperature difference across that bond. The law of current conservation was then applied at each point of the lattice, yielding a set of equations relating the potential at each point to the total applied potential and temperature difference across the lattice. This series of equations was solved by calculating the potential at each point as a function of its neighbors, and iterating this process through the entire lattice.

Several different methods were employed to assign the activation energies of each lattice point. One method was to select a value from a Gaussian or uniform distribution randomly for each point, with no spatial correlation in the activation energies of neighboring points. Another method introduced spatial correlations by first picking a random activation energy for each point, and then averaging each

point with its nearest neighbors, using periodic boundary conditions. The averaging process could be repeated any number of times to set longer and longer length scales for the spatial correlations. For both these methods, the standard deviation of the distribution of activation energies was used as a measure of the disorder. Since negative activation energies (resulting in local conductivities that decrease with increasing temperature) would be unphysical, all bond activation energies were required to be greater than or equal to zero for both distribution types. After the lattice was generated, the conductivity and thermopower of the entire lattice were calculated for several different temperatures, usually in the range of 300–450 K, which is the typical temperature range for our experimental measurements. The calculated values from all of the selected temperatures were fit to Eqs. (2) and (3) to find the activation energies of the thermopower and conductivity, respectively.

Figure 5(a) shows a sample lattice of the type used for calculations, where the gray scale indicates the activation energy at each point. This lattice was generated using the nearest-neighbor averaging method (performing the averaging process twice) for an average activation energy of 0.4 eV and a distribution width of 0.1 eV. Figure 5(b) is a plot of the same lattice, where now the current flow that results when an external potential is applied across the top and bottom of the lattice is shown, using a gray scale to indicate the logarithm of the current density passing through each lattice point. The brighter regions correspond to sections with a higher current density. The current tends to form filaments which pass through areas of the lattice that have relatively low activation energies. The image of the thermopower [Fig. 5(c)] is harder to interpret. This figure shows the thermoelectric voltage (divided by ΔT) at each point of the lattice, after subtracting off the uniform gradient that would result from a homogeneous sample with the same total thermopower. This subtraction is important since the deviations from a uniform gradient are in fact quite small, and a plot of the actual values of the voltage would appear to be uniform. In this picture, the top of the lattice is at the higher temperature. Finally, in Fig. 5(d) a gray-scale image of the thermoelectric charge distribution of the random resistor lattice is shown, obtained by differentiating the thermoelectric voltage of Fig. 5(c).

To examine the behavior of these quantities on a more detailed level, Fig. 6 shows the variations for the column indicated by the arrows in Fig. 5, where position 1 corresponds to the top row of the picture and position 40 represents the bottom row. Figure 6(a) compares the current density with the activation energies. It can be seen that the regions of high activation energy generally have a small current flow, although the current density remains high near the local maximum in the activation energy at row position 25 since the activation energies of the surrounding regions of the lattice are even higher, as seen in Fig. 5(a). Figure 6(b) compares the activation energies with the thermoelectric voltage [adjusted as in Fig. 5(c)], while Fig. 6(c) compares the activation energies with the thermoelectric charge density. Although the net current across the sample must be zero for the thermopower, there can be small circulating currents within the sample. There is generally a dipolelike buildup of charge across regions of high activation energy, with the negative charge near the high-temperature end. This can be

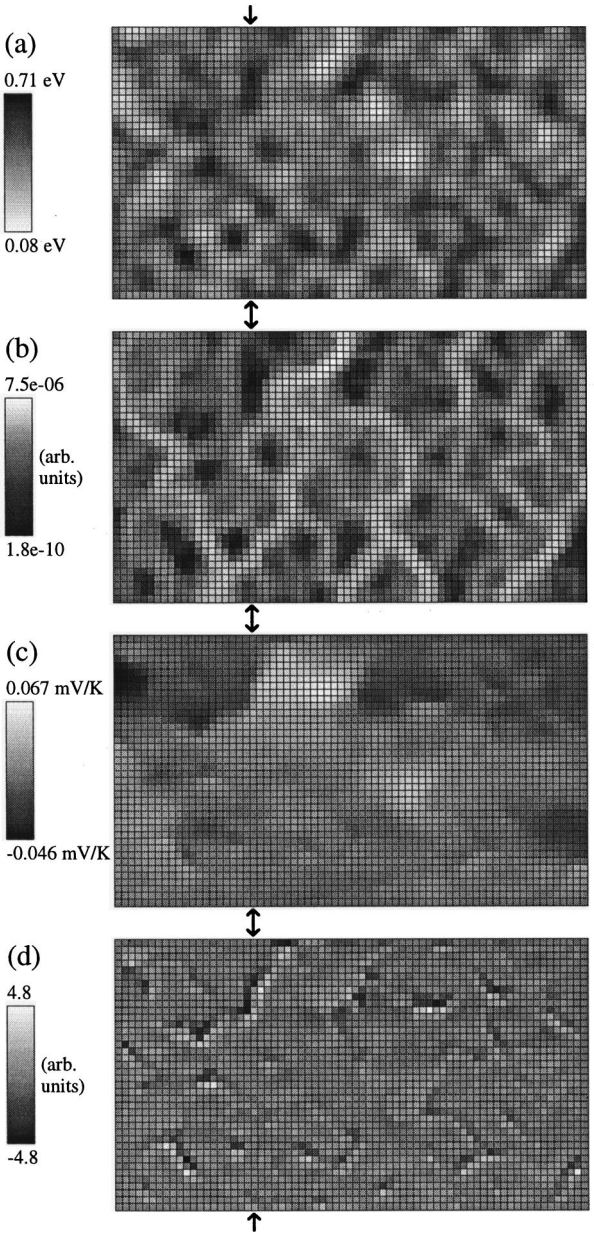

FIG. 5. Representative images from the random resistor lattice simulation indicating (a) activation energies; (b) current density (with a logarithmic gray scale); (c) deviation of the thermoelectric voltage from a uniform gradient, as described in the text; and (d) thermoelectric charge density. Images (b), (c), and (d) were calculated for a temperature of 400 K.

seen by comparing Figs. 5(a) and 5(d), and is more easily observed in Fig. 6(c) in the range of row positions 6–12, and to a lesser extent near row positions 25 and 40. This charge buildup will contribute to the circulating currents, which will act to reduce the value of the overall thermopower to less than that expected based upon the average activation energy.

As in the experimental measurements, the simulations find that the conductivity has a higher activation energy than the thermopower. For example, the lattice shown in Fig. 5 has activation energies of 0.392 eV for the conductivity and 0.266 eV for the thermopower. For both distribution types, we find that the activation energy difference depends strongly on the disorder in the lattice (as reflected by the

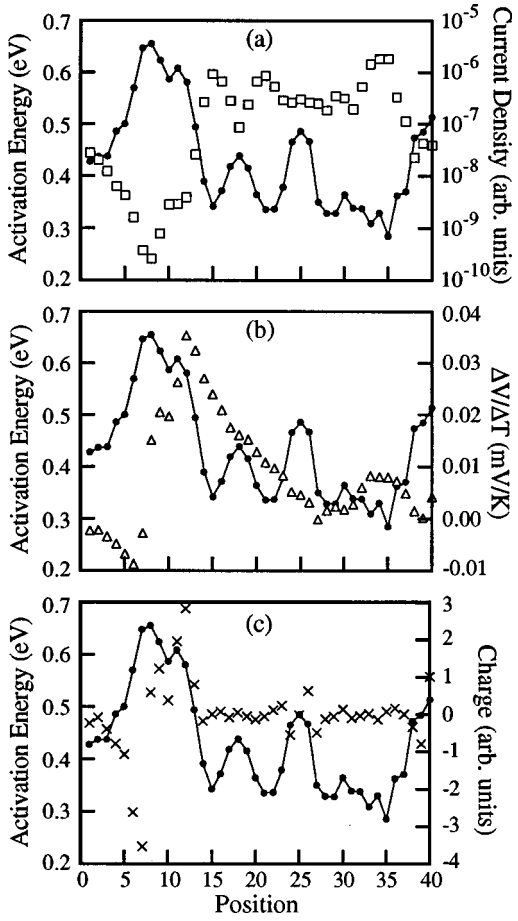

FIG. 6. Plots of data from a single column of the resistor lattice (marked with arrows in Fig. 5) as a function of row position. (a) Comparison of the activation energies (solid circles) and current density (open squares). (b) Comparison of the activation energies (solid circles) and thermoelectric voltage deviation (open triangles). (c) Comparison of the activation energies (solid circles) and thermoelectric charge density (crosses). The horizontal axis is the same for all three graphs.

width of the local activation energy distribution) but has no significant dependence on the average energy of the distribution. We also find that the activation energy of the conductivity decreases slightly as the disorder is increased (keeping the average activation energy constant), as previously seen in the simulations of Overhof and Beyer.[3] The wider distribution of activation energies provides more pathways with smaller barriers, leading to this small decrease of the conductivity activation energy. Figure 7 shows the activation energy difference as a function of the disorder in the lattice when the average lattice energy is 0.4 eV, for the uncorrelated Gaussian (nearly identical to E_Δ for the uniform distribution) and for the spatially averaged distributions. This figure shows that as the range of local activation energies widens, reflecting greater disorder in the resistor network, the bulk conductivity and thermopower activation energy difference similarly increases. The lattice dimensions used for these calculations were 120 points wide (transverse to the contacts) by 60 points across, and the results were obtained by averaging the activation energies calculated for ten lattices for each distribution. By comparing results from various lattice sizes, we have determined that finite size effects are not important for lattices of approximately 20×20 points or larger, unless the nearest-neighbor averaging procedure produces spatial correlations on length scales near the lattice size.

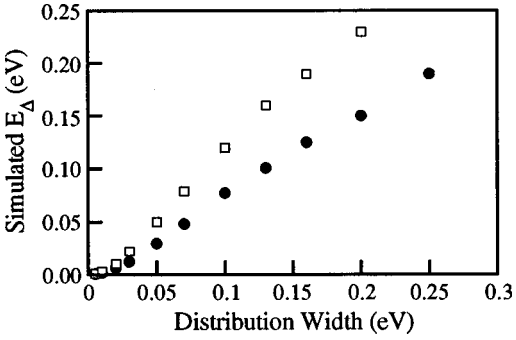

FIG. 7. Plot of simulated E_Δ from the resistor lattice as a function of the width of the activation energy distribution, for the Gaussian distribution (solid circles), and the nearest-neighbor-averaged distribution (open squares).

V. DISCUSSION

The computer simulations reported in Sec. IV are similar to those of Overhof and Beyer,[3] in that long-range fluctuations in the value of the mobility edge resulted in a difference between the conductivity and thermopower activation energies, with increased disorder resulting in larger values of E_Δ (see Fig. 7). Our simulations demonstrate that non-Coulombic disorder can result in reasonable values of E_Δ from realistic disorder levels, even for spatially uncorrelated disorder, unlike the results of Overhof and Beyer.[3] It may be that the small size of their three-dimensional lattice adversely affected their results and conclusions. The fact that the disorder of the network need not be due to Coulombic potential fluctuations supports the idea that long-range structural disorder can affect the electronic properties, and may be partially responsible for the observed values of E_Δ.

The results described in the present paper indicate that compositional heterogeneities associated with gross hydrogen microstructure can affect the macroscopic electronic properties of *a*-Si:H. The electrical current resulting from an external applied bias will flow mainly in those regions of the film with lower local activation energies, as in the computer simulations of Sec. IV. The energy landscape near the conduction-band edge would therefore resemble the ''Alpine model'' proposed by Fritzsche in 1971 (Ref. 23) in a very different context, with electrical conduction being described in terms of classical percolation channels which would carry the majority of the electrical current. This is not to say that in amorphous silicon conduction occurs at a percolation threshold. At higher energies above the conduction-band edge the sections which carry current are more interconnected and have a lower resistance due to their greater effective volume. The notion that the current in amorphous silicon occurs primarily at a ''transport energy'' which reflects the competition between a decreasing occupation function and an increasing electronic mobility at higher energies was introduced by Monroe in 1985 (Ref. 24), and has been generalized here to the case of inhomogeneous current filaments whose conductance increases with temperature.

We close by considering the implications of long-range

disorder induced by compositional morphology on the notion of a mobility edge. The results reported here and by other groups clearly indicate that the long-range inhomogeneities influence the electronic transport, with current flowing predominantly in the regions with lower activation energies. However, Mott argued that localized states and extended states cannot coexist at the mobility edge, for this would imply that $\sigma(E_C)$ would be both zero and nonzero at $T = 0$ K. The relevance of this argument has been challenged by others, who point out that this is only a concern for degenerately doped semiconductors, and that even in this situation, as for ceramic-metal alloys, the conductivity would either be metallic or insulating, depending on whether or not percolation channels of extended states spanned the dimensions of the semiconductor. The phase-coherence length for zero-temperature extended states in a highly disordered material which are not Bloch states (and for which the wave vector is not a valid quantum number) is not well understood, either theoretically or experimentally. Experimental studies of low temperature conduction in a degenerate amorphous semiconductor, possibly an *a*-Si:H based metal-oxide semiconductor field effect transistor in extreme bias, with care taken to avoid leakage currents, would provide important information on this fundamental question.

ACKNOWLEDGMENTS

We thank H. M. Dyalsingh for the original idea of studying the thermopower-conductivity activation energy difference as a function of deposition conditions and of studying correlations with the infrared absorption. We also thank P. W. West for assistance with sample processing. Infrared absorption spectra were measured at the NSF supported Center for Interfacial Engineering at the University of Minnesota. This research was supported by NSF Grant No. DMR-9424277 and the University of Minnesota.

[1] D. Emin, C. H. Seager, and R. K. Quinn, Phys. Rev. Lett. **28**, 813 (1972).
[2] G. H. Döhler, Phys. Rev. B **19**, 2083 (1979).
[3] H. Overhof and W. Beyer, Philos. Mag. B **43**, 433 (1981).
[4] R. A. Street, *Hydrogenated Amorphous Silicon* (Cambridge University Press, Cambridge, 1991).
[5] See, for example, B. I. Shklovskii and A. L. Efros, *Electronic Properties of Doped Semiconductors* (Springer-Verlag, Berlin, 1984).
[6] H. Overhof and P. Thomas, *Electronic Transport in Hydrogenated Amorphous Semiconductors* (Springer-Verlag, Berlin, 1989).
[7] W. Beyer, H. Mell, and H. Overhof, in *Proceedings of the 7th International Conference on Amorphous and Liquid Semiconductors*, edited by W. E. Spear (CICL, Edinburgh, 1977), p. 328.
[8] W. Beyer and H. Overhof, in *Hydrogenated Amorphous Silicon*, edited by J. Pankove, Semiconductors and Semimetals, Vol. 21C (Academic, Orlando, 1984), and references contained therein.
[9] J. A. Howard and R. A. Street, Phys. Rev. B **44**, 7935 (1991).
[10] H. Fritzsche, Appl. Phys. Lett. **65**, 2824 (1994).
[11] S. K. O'Leary, S. Zukotynski, and J. M. Perz, J. Appl. Phys. **72**, 2272 (1992).
[12] J. A. Reimer, R. W. Vaughan, and J. C. Knights, Phys. Rev. Lett. **44**, 193 (1980); J. Baum, K. K. Gleason, A. Pines, A. N. Garroway, and J. A. Reimer, *ibid.* **56**, 1377 (1986).
[13] G. D. Cody, B. Abeles, C. R. Wronski, R. B. Stephens, and B. Brooks, Sol. Cells **2**, 227 (1980).
[14] M. H. Brodsky, M. Cardona, and J. J. Cuomo, Phys. Rev. B **16**, 3556 (1977).
[15] G. Lucovsky, R. J. Nemanich, and J. C. Knights, Phys. Rev. B **19**, 2064 (1979).
[16] D. Jousse, E. Bustarret, and F. Boulitrop, Solid State Commun. **55**, 435 (1985); E. Bhattacharya and A. H. Mahan, Appl. Phys. Lett. **52**, 1587 (1988).
[17] H. M. Dyalsingh and J. Kakalios, Phys. Rev. B **54**, 7630 (1996).
[18] J. C. Knights and G. Lucovsky, CRC Crit. Rev. Solid State Mater. Sci. **21**, 211 (1980).
[19] J. C. Knights and R. A. Lujan, Appl. Phys. Lett. **35**, 244 (1979).
[20] J. Kakalios, R. A. Street, C. C. Tsai, and R. Weisfield, in *Amorphous Silicon Semiconductors—Pure and Hydrogenated*, edited by A. Madan, M. Thompson, D. Adler, and Y. Hamakawa, MRS Symposia Proceedings No. 95 (Materials Research Society, Pittsburgh, 1987), pp. 243–248.
[21] M. Cutler and N. F. Mott, Phys. Rev. **181**, 1336 (1969).
[22] W. Beyer, R. Fischer, and H. Overhof, Philos. Mag. B **39**, 205 (1979).
[23] H. Fritzsche, J. Non-Cryst. Solids **6**, 49 (1971).
[24] D. Monroe, Phys. Rev. Lett. **54**, 146 (1985).